

Synthesis, Characterization, and Photoinduced Antibacterial Activity of Porphyrin-Type Photosensitizers Conjugated to the Antimicrobial Peptide Apidaecin 1b

Ryan Dosselli,^{†,||} Cristiano Tampieri,[‡] Rubén Ruiz-González,[§] Sonia De Munari,^{‡,⊥} Xavier Ragàs,[§] David Sánchez-García,[§] Montserrat Agut,[§] Santi Nonell,[§] Elena Reddi,[†] and Marina Gobbo^{*,‡}

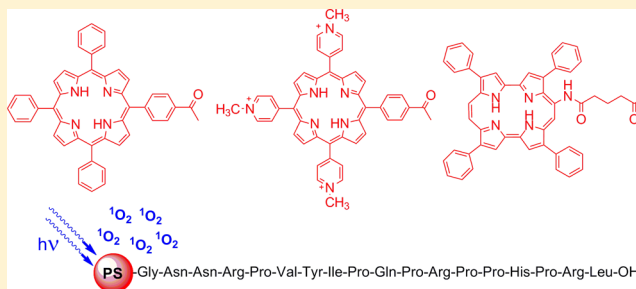
[†]Department of Biology, University of Padova, via U. Bassi 58/B, I-35121 Padova, Italy

[‡]Department of Chemical Sciences, University of Padova, via F. Marzolo 1, I-35131 Padova, Italy

[§]Institut Químic de Sarrià, Universitat Ramon Llull, Via Augusta 390, E-08017 Barcelona, Spain

S Supporting Information

ABSTRACT: Antimicrobial photodynamic therapy (aPDT) is an emerging treatment for bacterial infections that is becoming increasingly more attractive because of its effectiveness against multi-antibiotic-resistant strains and unlikelihood of inducing bacterial resistance. Among the strategies to enhance the efficacy of PDT against Gram-negative bacteria, the binding to a cationic antimicrobial peptide offers the attractive prospect for improving both the water solubility and the localization of the photoactive drug in bacteria. In this work we have compared a number of free and apidaecin-conjugated photosensitizers (PSs) differing in structure and charge. Our results indicate that the conjugation of per se ineffective highly hydrophobic PSs to a cationic peptide produces a photosensitizing agent effective against Gram-negative bacteria. Apidaecin cannot improve the phototoxic activity of cationic PSs, which mainly depends on a very high yield of singlet oxygen production in the surroundings of the bacterial outer membrane. Apidaecin–PS conjugates appear most promising for treatment protocols requiring repeated washing after sensitizer delivery.



■ INTRODUCTION

The global diffusion of new antimicrobial infections as well as the continuously increasing resistance of pathogens against many of the commonly used antibiotics imposes a considerable effort to develop alternative therapies to the use of classical drugs. In this area antimicrobial photodynamic therapy (aPDT; also termed photodynamic antimicrobial chemotherapy, PACT) represents a very promising strategy, particularly for the treatment of superficial and localized infectious diseases.¹ The PDT concept comprises the action of three components: a photosensitizer (PS), a light source of appropriate wavelength, and oxygen. The interaction between light and the PS leads to the generation of reactive oxygen species (ROS), e.g., singlet oxygen, by two possible mechanisms involving either electron-transfer (type I) or energy-transfer (type II) reactions.² These ROS are highly reactive and can damage a variety of cellular components, e.g., proteins, nucleic acids, and lipids, resulting in cytotoxicity.^{3–5} Advantages of aPDT over traditional antibiotics include a broad-spectrum activity, also against antibiotic-resistant species,⁶ and the lack of development of resistance mechanisms due to the multitarget process.^{7,8}

Porphyrins, commonly used as PSs in PDT, can efficiently kill Gram-positive bacteria, whereas only cationic PSs, or noncationic PSs in combination with agents that permeabilize the highly organized outer membrane of Gram-negative

bacteria, are able to kill Gram-negative species.^{9–11} An alternative approach to improve the susceptibility of Gram-negative bacteria to the photodynamic action of neutral porphyrins involves the covalent attachment of the PS to a polymer molecule containing basic amino groups¹² or, as we recently proposed, to a cationic antimicrobial peptide.¹³ Cationic antimicrobial peptides (CAMPs) are components of the innate defense of many organisms, and they are being considered a promising source of new antibiotics.¹⁴ In addition to exerting direct antimicrobial effects, many studies have documented their ability to affect various host cell activity and to have a key modulatory role in the innate immune response.^{44,45} Their overall positive charge ensures accumulation at the polyanionic microbial cell surfaces that contain acidic polymers, such as lipopolysaccharides, and wall-associated teichoic acids in Gram-negative and Gram-positive bacteria, respectively. Beyond the presence of several cationic amino acids, a substantial proportion of hydrophobic amino acid residues permit most of the CAMPs to fold into an amphipathic structure, which allows them to insert into the phospholipid bilayer of the cell membranes. After insertion, antimicrobial peptides act by either disrupting the physical

Received: October 17, 2012

Published: December 12, 2012

the peptide chain assembly. After cleavage and deprotection from the solid support, the conjugates **1c**, **1d**, **2c**, and **4e** were purified by reversed-phase HPLC and characterized by analytical HPLC, electrospray mass spectrometry, and UV-vis absorption spectroscopy.

Absorption and Fluorescence of the Conjugates. The spectroscopic and photophysical properties of the PSs and their conjugates were measured in aqueous and organic media and in cell suspensions to assess the structural and environmental effects as well as their correlation with antibacterial activity.

Methanol. Figures 2 and 3 show the absorption and fluorescence spectra of the free PSs and of their peptide conjugates in methanol. While the spectra of porphyrins are essentially insensitive to conjugation (panels A, C, and D), clear changes can be observed for the porphycene (panel B). In turn, the fluorescence quantum yield does not change appreciably for the porphyrins, while it drops by ca. 50% for the porphycene (Table 1). Finally, all porphyrins show monoexponential fluorescence decay kinetics, and conjugation does not change the lifetime values either (Supporting Information, Figure S1A,C,D). Again, the situation is different for the porphycenes in that the conjugate **2c** shows biexponential kinetics unlike the free porphycene **2a** (Figure S1B), and on average the singlet state decays faster (Table 1).

Aqueous Solutions (PBS). Porphyrin **4b** is water-soluble as a consequence of its positively and negatively charged groups. It remains water-soluble after conjugation (**4e**) with small but clear shifts in the position of the Soret and Q absorption bands and changes in their relative intensities (Figure 2E). The fluorescence spectrum of **4b** shows a single, structureless broad band (Figure 3E), a behavior strikingly different from that in methanol but in line with that of the related tetracationic *meso*-tetrakis(*N*-methylpyridinium-yl)porphyrin (TMPyP).³² Conjugation to the peptide (**4e**) leads to partial recovery of the two well-resolved fluorescence bands observed in methanol. The fluorescence decay kinetics of **4b** is monoexponential, albeit with a lifetime much shorter than that in methanol. For the conjugate **4e** two decay components can be observed, whose lifetimes are close to those of **4b** in methanol and in PBS, respectively (Figure S1E, Supporting Information, and Table 1). The kinetics is independent of concentration over 3 orders of magnitude (Figure S2A and Table S1, Supporting Information).

On the other hand, porphyrin **1b** and porphycene **2a** are insoluble in water, and therefore, no fluorescence can be recorded in this solvent. Conjugation to the peptides (**1c**, **1d**, and **2c**, respectively) renders them water-soluble, but the spectroscopic and photophysical properties change substantially relative to those in methanol: the absorption spectra show broadening of the Soret band and loss of structure in the Q region (Figure 2F–H), and the fluorescence is dramatically quenched. In addition, the fluorescence spectra of **1c** and **1d** are slightly red-shifted (Figure 3G,H), and the decays are biexponential (Figure S1G,H, Supporting Information, and Table 1) and show a clear concentration trend (Figure S2B,C and Table S1, Supporting Information).

***E. coli* Suspensions.** The conjugate **4e** shows in cell suspensions the same absorption and fluorescence properties as it does in PBS (Figures 2I and 3I and Table 1). On the other hand, there are evident changes for conjugates **1c** and **1d** in cell suspensions relative to PBS, particularly in the absorption spectrum and in the fluorescence kinetics, which shows a third decay component not present in PBS or in methanol (Table 1).

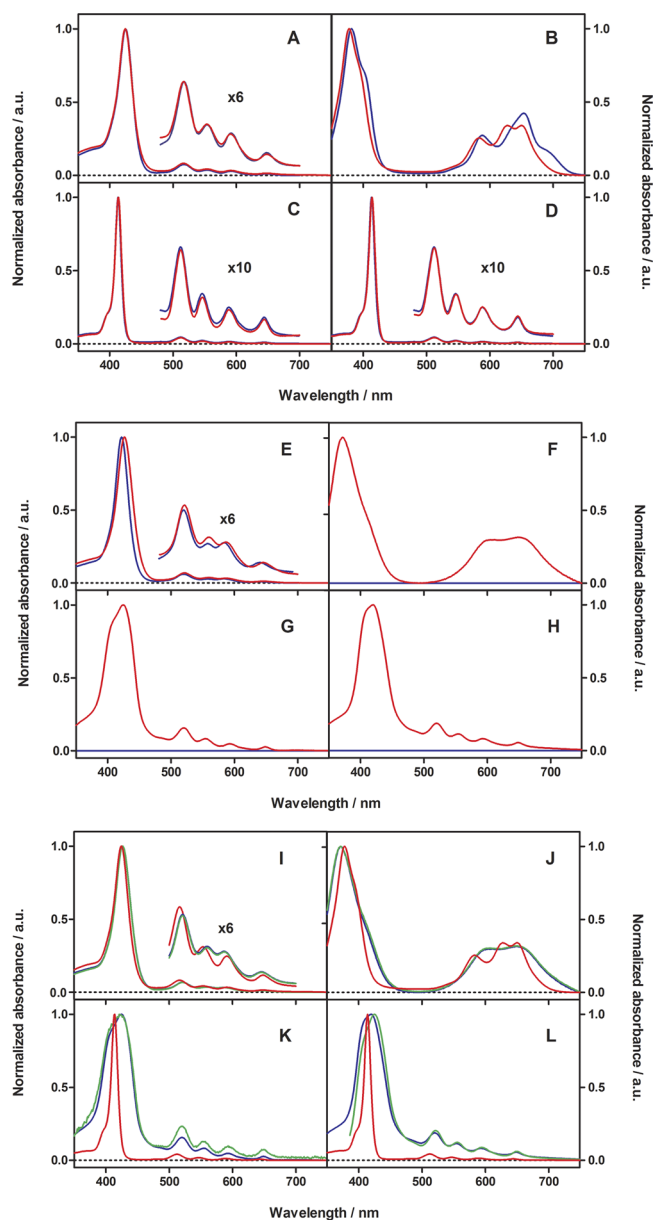


Figure 2. Absorption spectra in methanol (A–D), PBS (E–H), and *E. coli* suspensions (I–L), normalized to facilitate their comparison. The concentration is 5 μ M for all compounds. Methanol: (A) **4e** (red) and **4b** (blue); (B) **2c** (red) and **2a** (blue; dichloromethane as solvent); (C) **1d** (red) and **1b** (blue); (D) **1c** (red) and **1b** (blue). PBS: (E) **4e** (red) and **4b** (blue); (F) **2c** (red) and **2a** (blue); (G) **1d** (red) and **1b** (blue); (H) **1c** (red) and **1b** (blue). *E. coli* suspensions (green): (I) **4e**; (J) **2c**; (K) **1d**; (L) **1c**. Spectra in methanol (red) and PBS (blue) are given for comparison.

Finally, the porphycene conjugate **2c** shows very similar absorption spectra in PBS and in *E. coli* suspensions (Figure 2J). However, while we could record no fluorescence in PBS, we were nevertheless able to observe extremely weak biexponential fluorescence decay in the cells (Figure 3, Figure S1J, Supporting Information, and Table 1).

Singlet Oxygen Production and Decay. All free and conjugated PSs were able to photosensitize the formation of $^1\text{O}_2$ in methanol as evidenced by its phosphorescence at 1275 nm. The quantum yields of $^1\text{O}_2$ production (Φ_{Δ}) were in the 0.6–0.7 range for the porphyrins and the 0.1–0.3 range for the

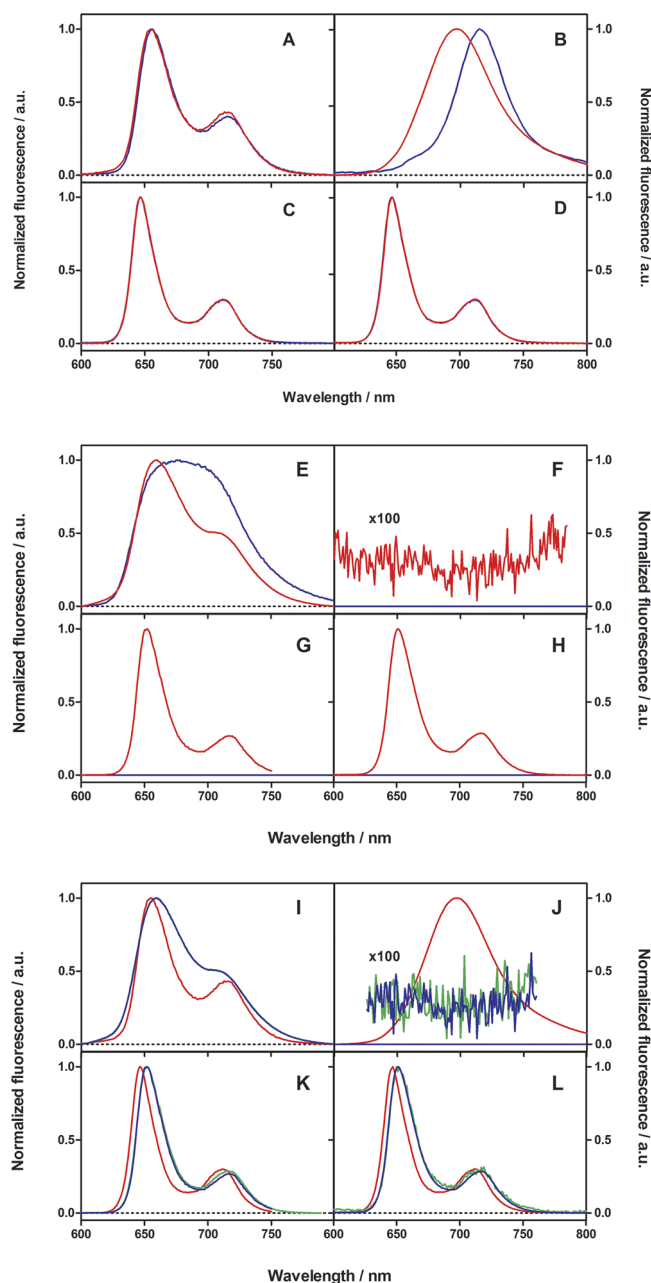


Figure 3. Emission spectra in methanol (A–D), PBS (E–H), and *E. coli* suspensions (I–L), normalized to facilitate their comparison. The concentration is 5 μM for all compounds. Methanol: (A) **4e** (red) and **4b** (blue); (B) **2c** (red) and **2a** (blue; dichloromethane as solvent); (C) **1d** (red) and **1b** (blue); (D) **1c** (red) and **1b** (blue). PBS: (E) **4e** (red) and **4b** (blue); (F) **2c** (red) and **2a** (blue); (G) **1d** (red) and **1b** (blue); (H) **1c** (red) and **1b** (blue). *E. coli* suspensions (green): (I) **4e**; (J) **2c**; (K) **1d**; (L) **1c**. Spectra in methanol (red) and PBS (blue) are given for comparison.

porphycenes (Table 2). The kinetics of $^1\text{O}_2$ production matched the results of laser flash photolysis experiments for the triplet PS decay (see the Supporting Information, Table S2). Likewise, an excellent match was found between the observed lifetime of $^1\text{O}_2$ and the literature values. In PBS, only porphyrins **4b** and **4e** retained their high ability to produce $^1\text{O}_2$; all other compounds experienced a decrease of the Φ_Δ value by 20–30-fold (porphyrins **1c** and **1d**) or even 100-fold (porphycene **2c**; Table 2). Inspection of the kinetics of $^1\text{O}_2$

(Figure S3, Supporting Information) reveals that production of singlet oxygen by conjugate **4e** is as fast as that by the free porphyrin **4b** (Table 2), yet for the conjugates **1c**, **1d**, and **2c** it is 1 order of magnitude slower. On the other hand, the lifetime of $^1\text{O}_2$ for all conjugates in deuterated PBS is shorter than the value expected in this solvent (67 μs),³⁴ which is actually observed only for the free porphyrin **4b**. When *E. coli* suspensions were studied, the $^1\text{O}_2$ signals showed essentially the same pattern as that in PBS solutions (Figure S4, Supporting Information, and Table 2).

Circular Dichroism (CD) Studies. The conformational properties of the conjugates were investigated by CD spectroscopy in different environments, including water and membrane-mimicking solvents, and compared to those of the parent peptide. As a consequence of the high proline content (6 out of 18 residues), in water apidaecin assumes a prevalently disordered, extended structure (Figure 4A), and in membrane-mimicking environments it exists as a mixture of conformers with a high percentage of nonrepetitive bent structures, most probably β -turns (Figure 4C,D).^{23,25} The CD spectra of the conjugates in water are characterized by a broad negative band around 200 nm, much more intense for those with the cationic porphyrin than for those with the neutral PS (Figure 4A). Moreover, **1c** and **2c** showed a split Cotton effect in the Soret band region (Figure 4B), indicating that porphyrins are chirally oriented and close to one another in space.³⁵ These results suggest that while **4e** can assume in water a fully extended structure, conjugates **1c** and **2c** show the tendency to form aggregates with the peptide chain probably folded over the hydrophobic porphyrin platform³⁶ and the porphyrins close to one another to reduce the exposure to the solvent. Aggregation was confirmed by a change in the UV spectra of these conjugates moving from methanol to water. In organic solvent (2,2,2-trifluoroethanol, TFE) and in the presence of SDS micelles, the CD spectrum of the conjugates is similar to that of the parent peptide, with a broad band at 202 nm, a shoulder at 220 nm, and comparable intensities (Figure 4C,D). This suggests that in membrane-mimicking environments the conformational preferences of the peptide are minimally affected by the intramolecular interactions with the PS.

Photoinactivation of *E. coli*. To determine the photosensitizing efficiency of our PSs and peptide–PS conjugates against Gram-negative bacteria, *E. coli* suspensions were incubated in the dark for 60 min with different concentrations (1.5, 5, 10, and 15 μM) of the agents and then illuminated (light dose of 36 J/cm^2 of red light for **2a** and **2c**, 13.5 J/cm^2 of blue light for all other compounds) with or without washings. At the concentrations used, apidaecin alone did not cause any decrease of *E. coli* survival,¹³ as did its C-terminal segment **1d**, in both the dark and light conditions (Table S3, Supporting Information). In addition, neither **1b** nor **2a** caused any bacteria photokilling in their unconjugated form. All conjugates exhibited markedly concentration-dependent abilities to kill *E. coli* under illumination with an efficiency that largely depended on the type of conjugate (Figure 5A). Indeed, considering the unwashed samples, **4b** and **4e** caused complete killing of bacteria at 5 and 10 μM concentrations, respectively, while all other agents were considerably less potent and at 15 μM reduced the survival of *E. coli* by 4 log at maximum. Moreover, it is interesting to notice that **1c** was slightly more efficient than **1d** and caused a bacterial mortality similar to that of **2c**. However, when illumination was carried out after three washings of the cells to remove the unbound PS (Figure 5B;

Table 1. Fluorescence Properties of the Peptide Conjugates and Model Compounds in Methanol, PBS, and *E. coli* Suspensions (Fractional Amplitudes in Parentheses)

compd	$\lambda_{F,max}/nm$			Φ_F		τ_S/ns		
	MeOH	PBS	<i>E. coli</i>	MeOH ^a	PBS ^b	MeOH	PBS	<i>E. coli</i>
1b	647	ns ^c		0.040	ns	10.1	ns	
1c	647	651	651	0.050	0.006	9.8	10.7 (0.82) 3.1 (0.18)	10.5 (0.46) 7.5 (0.33) 3.1 (0.21)
1d	646	652	652	0.044	0.006	9.8	6.1 (0.61) 2.6 (0.39)	5.9 (0.11) 4.9 (0.48) 2.5 (0.41)
2a	715	ns		0.030 ^d		1.46 ^d		
2c	697			0.016	<0.0001	0.9 (0.94) 9.6 (0.06)		0.9 (0.75) 5.2 (0.25)
4b	656	675		0.022	0.008	7.9	4.2	
4e	655	660	660	0.024	0.018	8.1	4.2 (0.49) 7.1 (0.51)	4.2 (0.48) 7.1 (0.52)

^aCresyl violet as standard ($\Phi_F(\text{methanol}) = 0.54$).³¹ ^bTMPyP as standard ($\Phi_F(\text{PBS}) = 0.017$).⁹ ^cNot soluble. ^dIn toluene.

Table 2. Kinetics of Singlet Oxygen Production (Φ_Δ) and Decay (τ_Δ) of the Peptide Conjugates and Model Compounds in Air-Saturated Methanol, PBS, and *E. coli* Suspensions

compd	Φ_Δ		$\tau_\Delta/\mu s$		
	MeOH ^a	PBS ^b	MeOH ^c	PBS ^d	<i>E. coli</i> ^e
1b	0.63	ns ^f	9.8	ns	
1c	0.70	0.020	9.8	3.0	2.3
1d	0.66	0.036	9.5	43 ^g	
2a	0.26 ^h	ns		45 ^g	
2c	0.14	0.001	9.8	ns	
4b	0.69	0.73	9.6	42 ^g	3.6
4e	0.67	0.89	9.6	60 ^g	3.6
				36 ^g	

^aTMPyP as standard ($\Phi_\Delta(\text{methanol}) = 0.74$).³ ^bTPPS as standard ($\Phi_\Delta(\text{water}) = 0.69$).³ ^cLiterature value 10.4 μs .³³ ^dLiterature value 3.3 μs in PBS and 67 μs in D-PBS.³³ ^eIn PBS. ^fNot soluble. ^gIn D-PBS. ^hToluene as solvent.

Figure S5, Supporting Information), only **1d** retained an efficacy similar to that observed in unwashed samples, while all other PSs were considerably less potent. In particular, the loss of efficacy of **4b** and **4e** in killing bacteria was drastic, with a decreased killing ability of 6 log at the 10 μM concentration. On the other hand, **1c** and **2c**, which were less photoactive without washings, were less hampered by the washing treatment. We also studied the photoinactivation of *E. coli* as a function of the incubation times and using a concentration of 5 μM for **4b** and **4e** and 10 μM for all other compounds (Figure S6, Supporting Information). The results showed that the time of dark incubation of the cells with the PSs and their conjugates before irradiation does not affect to a great extent the photokilling efficiency of *E. coli*. Incubation times ranging from 15 to 120 min gave very similar decreases of bacterial survival when irradiation was carried out leaving the unbound PS in solution. Only with **4b** and **4e** was the photoinactivation ability slightly improved by increasing the incubation time, but this effect was lost after the repeated washing treatment.

Photoinactivation of MRSA. The photoinactivation of MRSA was studied by using the same experimental approach

used for *E. coli*. Contrary to *E. coli*, both **1b** and **4b** were highly photoactive against MRSA; they caused complete killing of unwashed bacteria at, respectively, 50 nM and 0.5 μM concentrations (Figure 6A). These findings are in agreement with the well-known susceptibility of Gram-positive bacteria to many cationic and neutral PSs. However, the photoactivities of the two porphyrins were differently affected by the washing treatments: **1b** did not show any appreciable change, while the potency of **4b** was dramatically reduced (Figure S7A, Supporting Information). Both **1b** and **4b** lost part of their activity when conjugated to apidaecin or its C-terminal segment. In particular, at a 0.5 μM concentration the unconjugated porphyrins caused complete cell killing, while **4e**, **1c**, and **1d** caused only about a 3 log reduction of survival (Figure 6A). The washing of *S. aureus* before illumination did not appreciably reduce the killing efficiency of **1c** and **1d**, while it significantly affected that of **4e**, as was observed with *E. coli* (Figure S7A). **2a** and its apidaecin conjugate **2c** were less effective than the porphyrin counterparts, being active in the range of 1.5–15 μM , i.e., at 10-fold higher concentrations (Figure 6B). However, conjugation with apidaecin strengthened the action of the PS (Figure S7B). As for *E. coli*, also with *S. aureus* the photoinactivation experiments were performed as a function of the incubation time, and no major differences in the efficiency of *S. aureus* photoinactivation with conjugated and unconjugated PSs were found by changing the incubation times from 15 to 120 min (Figure S8, Supporting Information).

Uptake Experiments. Flow cytometry experiments were carried out to evaluate the interaction of the PSs (free or conjugated to apidaecin) following incubation with *E. coli* and *S. aureus* cells under the same experimental conditions as in the photoinactivation experiments. The measurements showed that **1b** does not associate with *E. coli* cells very efficiently. As shown in Figure 7, after incubation with 5 μM **1b**, only a small fraction of *E. coli* cells exhibited a fluorescence signal higher than the basal value in both washed and unwashed cells. On the contrary, MRSA cells incubated with **1b** exhibited a fluorescence signal whose intensity was orders of magnitude higher than the background signal, suggesting efficient porphyrin association/binding either before or after the washings. The conjugation of **1b** to apidaecin or its C-terminal segment did not affect to a great extent the association of **1b** with MRSA, while it increased the association with *E. coli*, as

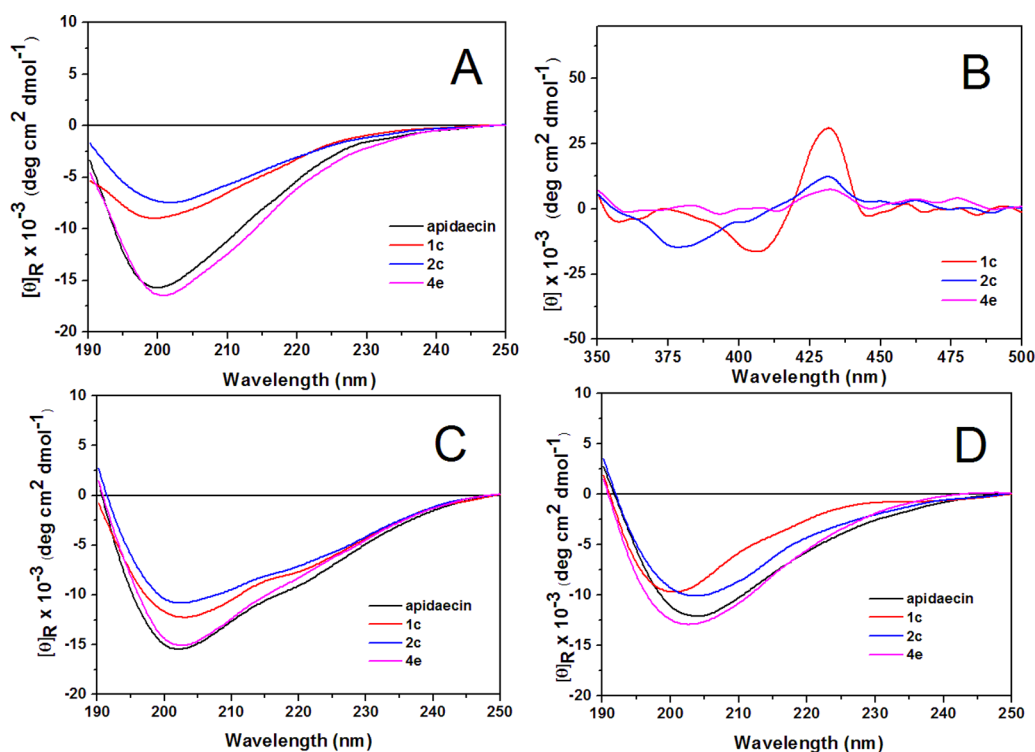


Figure 4. CD spectra of apidaecin and its conjugates in 10% methanol (A, amide region; B, Soret region), TFE (C), and 30 mM aqueous SDS (D). The peptide concentration is 10 μ M.

clearly shown by the higher fluorescence signals exhibited by a large fraction of cells incubated with **1c** and **1d**. Both free and apidaecin-conjugated **4b** did not appreciably interact with *E. coli* since only in unwashed cells was the measured mean fluorescence intensity slightly higher than the background signal. Similar results were observed with MRSA cells, suggesting that **4b** and its conjugate exhibit a very poor ability to interact with both Gram-positive and Gram-negative bacteria.

DISCUSSION

In our previous paper¹³ we have already shown that the conjugate **1c** is endowed with antibacterial activity following light activation. In this paper we have extended our investigations to other PS–apidaecin conjugates, containing either a neutral porphycene or a cationic porphyrin (respectively **2a** and **4b** in Figure 1) to assess the effects of structural modifications. Porphycene, a structural isomer of porphyrin, was chosen for its larger absorption coefficients in the red part of the spectrum, where light can deeply penetrate into tissues.³⁷ Because positively charged PSs are effective in PDT against Gram-negative bacteria without the addition of outer-membrane-disrupting agents,³⁸ we hypothesized that a conjugate between apidaecin and a cationic porphyrin could further promote the uptake of the PS in Gram-negative bacteria, thereby reducing the minimum effective dose. Moreover, to establish whether the antimicrobial peptide is able to direct the PS against specific bacterial targets, we also synthesized a conjugate between porphyrin **1b** and a short cationic peptide (PRPPHPRL) corresponding to the C-terminal segment of apidaecin. Although the mode of action of apidaecin has not been determined in detail, several points of evidence suggest that this peptide enters *E. coli* cells by a non-pore-forming mechanism and, once inside the cell, interacts

with components of the protein synthesis machinery, impairing protein synthesis and folding.^{17,18} The full-length apidaecin sequence is very important, and the C-terminal octapeptide does not possess any antibacterial activity,²¹ nor is it able to translocate a fluorescent cargo into bacterial cells.²⁴ Thus, most probably, the conjugate with this cationic peptide (**1d**) can effectively bind to the bacterial cell wall without being able to reach the cytosol.

Efficient PSs for PDT must have appropriate photophysical properties, such as an intense red-light absorption band and a high quantum yield of generation of both the long-lived excited triplet state and cytotoxic ROS, in particular singlet oxygen, ¹O₂. To establish whether the peptide moiety negatively affects the PS photosensitizing efficiency, the porphyrin–peptide conjugates were submitted to a detailed photophysical characterization. The fluorescence properties and the singlet oxygen production ability of the peptide conjugates **1c–d** and **4e** in methanol (Tables 1 and 2) are essentially identical to those of free PSs, demonstrating that the peptide moiety exerts no influence on the PS photosensitizing efficiency in this solvent. Only in the case of porphycene **2a** did we observe changes in the absorption spectrum and a reduction by about 50% of the fluorescence quantum yield of the PS and in ¹O₂ production after conjugation to the peptide, which may be ascribed to interactions between the peptide and the macrocyclic core. The situation is different in an aqueous environment (PBS) where the photophysical data change considerably relative to those in methanol for all conjugates and particularly for those containing a neutral PS. The decrease in the fluorescence quantum yield, the concentration dependence of the fluorescence kinetics, and the slow kinetics of ¹O₂ production in **1c–d** and **2c** reveal the presence of intermolecular interactions, as observed also by CD spectroscopy.

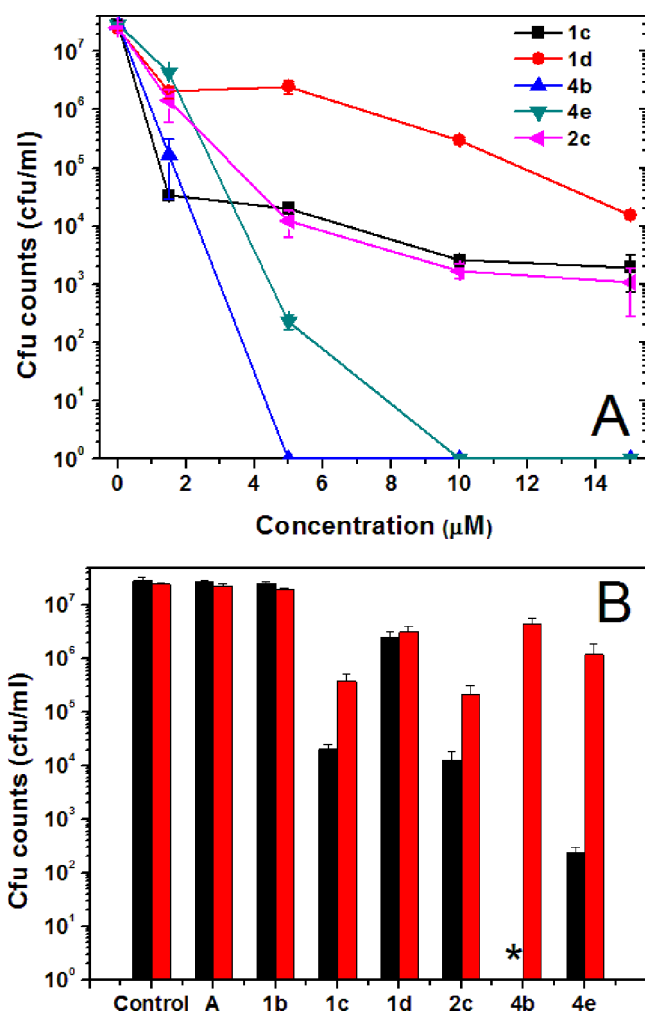


Figure 5. (A) *E. coli* photoinactivation with different concentrations (1.5–15 μM) of 2c, 1c, 1d, 4b, and 4e. *E. coli* cells were incubated for 60 min with the PS and irradiated with a fixed light dose (36 J/cm² of 600–750 nm red light for 2c, 13.5 J/cm² of 390–460 nm blue light for all other compounds). (B) *E. coli* photoinactivation with a 5 μM concentration of apidaecin or the tested PSs. Irradiation with a fixed light dose, as described above, was carried out without washing (black bars) or after three washings with PBS (red bars); the asterisk means a sterile solution.

copy (Figure 4B). Such interactions account also for the 20-fold lower production of ¹O₂ in PBS relative to methanol (Table 2).

Nevertheless, following illumination (with blue light for 1c–d and red light for 2c), the conjugates were phototoxic against *E. coli* cells, inducing a decrease of survival of 3–4 log at a 15 μM concentration (Figure 5). On the other hand, the unconjugated PS 2a was completely ineffective toward *E. coli* (data not shown), consistent with data previously reported for 1b¹³ and other neutral porphyrins, which are unable to diffuse through the highly organized outer membrane of Gram-negative bacteria.³⁹ Peptide conjugates 1c–d and 2c associate efficiently with *E. coli* cells, as suggested by the observation that repetitive washing of bacteria treated with conjugates, before illumination, caused only a moderate reduction of phototoxicity (Figure 5B; Figure S5, Supporting Information). In the case of 1c–d this is also supported by the flow cytometry results (Figure 7). Porphycene was not fluorescent enough for cytometry studies, but the detection of fluorescence by time-resolved techniques in the *E. coli* suspensions, but not in PBS (Table 1), must be taken as proof of binding. A deeper understanding of the type of binding/association of 1c–d to *E. coli* cells was obtained by analyzing the fluorescence decay kinetics: unlike PBS or methanol, three decay components were observed in cell suspensions, which suggest multiple binding sites (Table 1). The match between two of the three observed lifetimes with those detected in PBS indicates that one binding site is located in an aqueous-like environment. Thus, the third decay component suggests that an additional binding site exists where the conjugates experience a less hydrophilic environment.

However, the phototoxicity and the photophysical and flow cytometry results for the apidaecin conjugate 1c and its truncated analogue 1d are so similar that it is difficult to propose a different localization of these conjugates in *E. coli* cells. Most probably both conjugates can diffuse through the outer membrane and localize in different environments, but since the C-terminal apidaecin fragment is unable to translocate a PS across the cytoplasmic membrane, we are led to conclude that the apidaecin conjugate is also not able to reach the bacterial targets of apidaecin in cytosol.

The conjugate between the cationic porphyrin 4e and apidaecin possesses a +6 net positive charge, well-distributed along the whole molecule, that is expected to discourage the aggregation phenomena observed in conjugates 1c and 2c. In

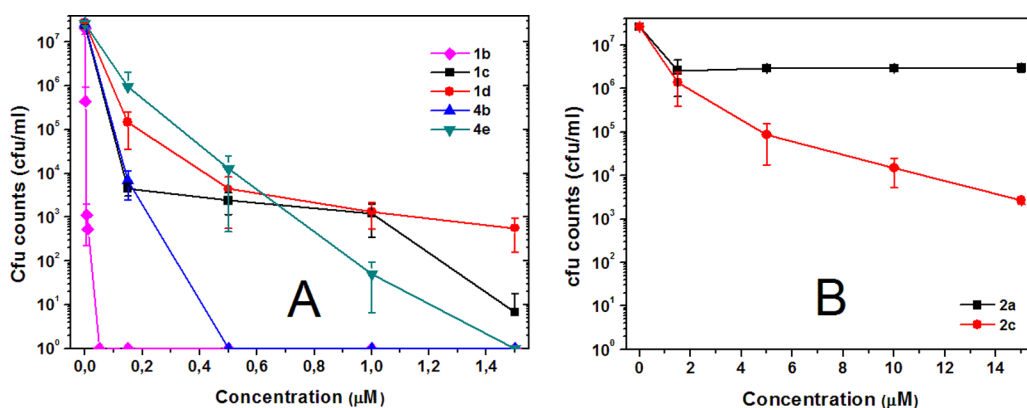


Figure 6. MRSA photoinactivation with different concentrations of (A) 1b, 1c, 1d, 4b, and 4e (1 nM to 1.5 μM) and (B) 2b and 2c (1.5–15 μM). MRSA cells were incubated with the PS for 60 min and irradiated with a fixed light dose (36 J/cm² of 600–750 nm red light for 2b and 2c, 13.5 J/cm² of 390–460 nm blue light for all other compounds).

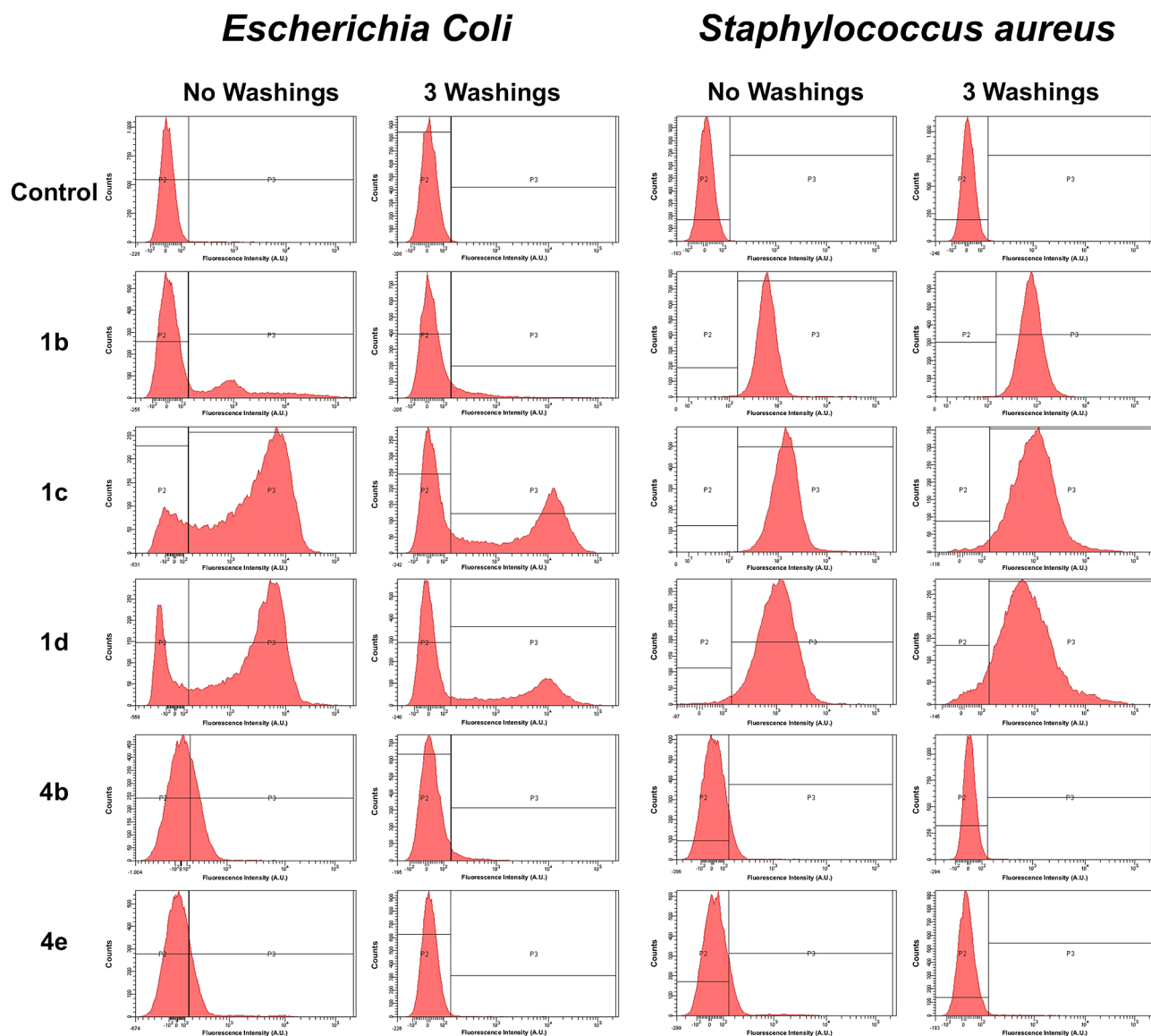


Figure 7. Uptake of the peptide conjugates and model PSs in *E. coli* and MRSA. The cells were incubated with the compounds for 60 min and then analyzed by flow cytometry. Concentrations of the compounds: 5 μM for *E. coli* and 1.5 μM for MRSA.

confirmation of this, the far-UV CD spectrum of **4e** in water is very similar to that of the free peptide and no dichroic signal, indicative of porphyrin–porphyrin interactions, was detected in the Soret band region (Figure 4 A,B). Aggregation can also be ruled out by the lack of concentration effects on the decay kinetics (Figure S2A and Table S1, Supporting Information). It can therefore be safely concluded that the major differences observed between **4b** and **4e** (Table 1) are due to interactions between apidaecin and the porphyrin within the conjugate. Comparison of the fluorescence spectrum, quantum yield, and kinetics for **4b** and **4e** reveals that two populations of conjugates coexist, in which the porphyrin is either exposed to water or shielded from it by the peptide. This conclusion is consistent with the well-known solvent-polarity effects on the fluorescence of tetrapyrrolic porphyrins.³² Nevertheless, the production of $^1\text{O}_2$ was very high in PBS, comparable to or even higher than that in methanol (Table 2). In fact, the conjugate **4e** caused total photokilling of *E. coli* cells at a concentration (10 μM) at which **1c** induced a strong (4 log) but incomplete reduction of cell survival (Figure 5A). The cationic porphyrin

4b proved to be even more potent than its apidaecin conjugate **4e** (Figure 5A). The $^1\text{O}_2$ lifetime data in Table 2, particularly in deuterated PBS, indicate that apidaecin is able to quench $^1\text{O}_2$. Thus, because $^1\text{O}_2$ molecules are generated in the vicinity of apidaecin, some of them will be quenched by the peptide during their lifetime rather than by cell components.

The washing of the cells before illumination, to remove the unbound or weakly associated PS, caused a tremendous reduction of photokilling of *E. coli* cells, and under these conditions **4b** became the least efficient PS (Figure 5B; Figure S5, Supporting Information). Flow cytometry measurements showed that only unwashed cells exhibited red fluorescence slightly above the background after incubation with these compounds (Figure 7). Thus, the results indicate that **4b** and **4e** associate very weakly with *E. coli* cells and the killing of unwashed cells is caused mainly by singlet oxygen generated by the PS molecules not associated with or loosely associated with the bacteria. Several reports of PDT on Gram-negative bacteria have pointed out that if singlet oxygen can be generated in sufficient quantities near the bacterial outer membrane, it will

be able to diffuse into the cell to inflict damage to the vital structure.^{1,40} Our photophysical data thus support this hypothesis.

Testing the above PS against MRSA reveals a number of differences relative to *E. coli*. First, except for the porphycene, the concentration needed to inactivate bacteria was 1 order of magnitude lower. Interestingly, the porphycene conjugate was almost equally active against both kinds of bacteria. The higher susceptibility of Gram-positive bacteria to photodynamic damage has long been known for a large number of PSs.⁴¹ Second, it is interesting to recall that washings did not appreciably remove **1b** and its conjugates (**1c** and **1d**) from the cells (Figure 7), nor did it decrease the photodynamic inactivation of MRSA (Figure S7, Supporting Information). In addition, the nonconjugated porphyrin **1b** was the most active PS. This probably can be related to its more hydrophobic character, which helps in penetration of the cell wall and the cytoplasmic membrane of Gram-positive bacteria. The porphycene **2a** was probably too hydrophobic, and its strong aggregation in the external medium prevented cell entrance. Concerning PSs **4b** and **4e**, the observations are similar to those of *E. coli*: the nonconjugated PS **4b** is more active than **4e** on account of its lower ability to quench ¹O₂, and both lose their activity after washings due to the very poor binding to the bacterial cells (Figure 7).

CONCLUSIONS

The search for more effective antimicrobial PSs has led to a number of strategies. Among them, binding to an antimicrobial peptide offers the attractive prospect of enhancing both the water solubility of the PS and the efficiency of the PDT treatments through a synergistic effect. In this work we have compared a number of free and apidaecin-conjugated PSs differing in structure and charge. Our results confirm previous findings that the conjugation of per se ineffective highly hydrophobic PSs to a cationic peptide produces a photosensitizing agent effective against Gram-negative bacteria. MRSA are even more susceptible to the action of conjugates, which produce the same reduction of bacterial growth at one-tenth the concentration. The apidaecin ability to penetrate Gram-negative bacteria is unfortunately lost after conjugation to a bulky PS, but the amphiphilic character conferred by the peptide enforces the binding of the PS to the bacterial outer membrane. Apidaecin-PS conjugates appear most promising for treatment protocols requiring repetitive washing after sensitizer delivery, where the most active cationic PSs, such as **4b** and its apidaecin conjugate **4e**, are rapidly washed out. On the other hand, apidaecin cannot improve the phototoxic activity of the cationic porphyrin, which is mainly determined by a very high yield of singlet oxygen production in the surroundings of the bacterial outer membrane.

EXPERIMENTAL SECTION

General Methods. All chemicals were commercial products of the best grade available, and unless otherwise indicated, they were used directly without further purification. The starting porphyrins, 5-(4-carboxyphenyl)-10,15,20-triphenylporphyrin (**1b**),⁴² 9-(glutaric methyl esteramide)-2,7,12,17-tetraphenylporphycene (**2a**),²⁹ and 5-(4-carboxyphenyl)-10,15,20-tris(4-pyridyl)porphyrin (**3b**) and its tris-*N*-methylpyridinium iodide (**4b**),²⁸ were prepared according to literature procedures. 9-Fluorenylmethoxycarbonyl (Fmoc)-amino acids and all other chemicals for the solid-phase synthesis were supplied by Sigma-Aldrich. Fmoc-Leu-Wang resin was purchased from Novabiochem (Merck Biosciences). Analytical HPLC separations were carried out on

a Dionex Summit dual-gradient HPLC instrument, equipped with a four-channel UV-vis detector, using a Vydac 218TP54 column (250 × 4.6 mm, 5 μm, flow rate at 1.5 mL/min). Mobile phases A (aqueous 0.1% trifluoroacetic acid (TFA)) and B (90% aqueous acetonitrile containing 0.1% TFA) were used for preparing binary gradients. All analyses were carried out under gradient conditions (10–50% B in 20 min, except as otherwise indicated). All crude peptides were purified to 95% or more homogeneity for analytical and other experimental purposes. Semipreparative HPLC was carried out on a Shimadzu series LC-6A chromatograph, equipped with two independent pump units, a UV-vis detector, and a Vydac 218TP1022 column (250 × 22 mm, 10 μm, flow rate at 15 mL/min). Elutions were carried out by the same mobile phases described above. All the purified peptides were analyzed again by HPLC and HRMS. Mass spectral analyses were carried out on a Mariner API-TOF workstation (PerSeptive Biosystems Inc.), operating with ESI techniques in positive mode. NMR spectra were recorded on a Varian Gemini 300 spectrometer (300 and 75.5 MHz for ¹H and ¹³C, respectively). UV-vis spectra were recorded at rt on a Shimadzu UV-2501PC spectrophotometer or on a Lambda 5 spectrophotometer (Perkin-Elmer), in 0.1 or 1 cm quartz cells.

Chemical Synthesis. 19-Glutaramide-2,7,12,17-tetraphenylporphycene (**2b**). A 44 mg (0.1 mmol) sample of **2a** was dissolved in 14 mL of THF and combined with 14 mL of methanol, and 9 mL of 4 N aqueous sodium hydroxide was added dropwise with stirring at rt within 5 min. The reaction was stirred for an additional 45 min, neutralized, and then precipitated under acidic conditions with the complete addition of 50 mL of ice-cold 5% acetic acid. The flaky precipitate was filtered, washed with water and then with water/methanol (1:1), and dried. The title compound was obtained in the form of a dark green powder. Yield: 27 mg (70%). ¹H NMR (400 MHz, DMSO-*d*₆): δ = 12.10 (br s, 1H), 10.96 (s, 1H), 10.08 (s, 1H), 10.07 (s, 1H), 10.05 (s, 1H), 9.93 (d, *J* = 12, 1H), 9.91 (d, *J* = 12, 1H), 9.85 (s, 1H), 9.82 (s, 1H), 8.37 (m, 6H), 7.98 (d, *J* = 8, 2H), 7.88 (m, 5H), 7.74 (m, 5H), 7.60 (m, 2H), 4.29 (s, 1H), 3.93 (s, 1H), 2.25 (t, *J* = 8, 2H), 2.16 (t, *J* = 8, 2H), 1.72 (q, *J* = 8, 2H). ¹³C NMR (100 MHz, DMSO-*d*₆): δ = 174.1, 171.9, 158.0, 144.7, 143.7, 142.8, 142.7, 141.3, 139.1, 137.7, 135.6, 135.4, 135.3, 134.8, 134.3, 133.3, 132.8, 131.1, 131.0, 130.3, 129.2, 129.2, 129.1, 128.0, 127.4, 127.1, 123.1, 125.0, 124.5, 116.0, 115.5, 113.9, 33.9, 33.06, 19.8. HRMS (ESI-TOF): *m/z* calcd for C₄₉H₃₈N₅O₃ 744.2969 [M + H]⁺, found 744.2970.

Synthesis of PS-Peptide Conjugates (General Procedure). The peptide sequences were prepared on an automated Advanced Chemtech 348Ω peptide synthesizer, on a 0.25 mmol scale, starting from Fmoc-Leu-Wang (substitution 0.6 mmol/g of resin). The *tert*-butyl group and 2,2,4,6,7-pentamethylidihydrobenzofuran-5-sulfonyl group were used to protect tyrosine and arginine side chains, respectively, and the trityl group to protect asparagine and histidine side chains. Fmoc deprotection was achieved with 20% piperidine in DMF (5 + 15 min). Couplings were performed in the presence of *O*-(benzotriazol-1-yl)-*N,N,N'*-tetramethyluronium hexafluorophosphate/*N*-hydroxybenzotriazole/*N,N*-diisopropylethylamine (reaction time 45–60 min), using an excess of 4 equiv of the carboxyl component. After the coupling of the last amino acid and removal of the Fmoc group, the resin was washed with DMF and CH₂Cl₂ and then dried under vacuum. The dried resins containing the protected amino acid sequences were used in the coupling reaction to the porphyrin derivatives. The H-peptide-resin (0.025 mmol) was swelled in DMF for 1 h and then washed with DMF. To the peptidyl resin was added 600 μL of a DMF-CH₂Cl₂ (1:1, v/v) solution containing 0.05 mmol of porphyrin (**1b**, **2b** or **3b**), 0.05 mmol of diisopropylcarbodiimide, and 0.05 mmol of 1-hydroxybenzotriazole. The reaction mixture was shaken overnight and then filtered to remove the excess of reagents. The resin was repeatedly washed with DMF and CH₂Cl₂, until the filtrate was colorless, and then dried under vacuum. Cleavage and deprotection was carried out by treatment of the resin with a mixture of TFA-triisopropylsilane-water (95:2.5:2.5 by volume) for 1.5 h at rt. The resin was filtered and washed with TFA, and the filtrates were combined and reduced under vacuum to a small volume. Addition of cold ether yielded a green precipitate, which was repeatedly washed with ether and dried under vacuum. The conjugates

1–3c and **1d** were purified by semipreparative HPLC (linear gradient 50–80% B in 20 min), and the fractions containing the conjugate were collected and lyophilized to yield the pure compound. The purity was $\geq 95\%$ as determined by analytical HPLC (isocratic 10% B for 3 min; linear gradient 10–90% B in 30 min). The conjugates were characterized as follows:

(**1c**) Yield: 75%. HPLC: $t_R = 22.0$ min. UV–vis (methanol): λ_{\max}/nm ($\log \epsilon/\text{M}^{-1} \text{cm}^{-1}$) 414 (5.48), 513 (4.05), 546 (3.70), 591 (3.45), 642 (3.35). HRMS: m/z calcd for $\text{C}_{140}\text{H}_{179}\text{N}_{36}\text{O}_{24}$ 2748.38 $[\text{M} + \text{H}]^+$, found 2748.39.

(**1d**) Yield: 80%. HPLC: $t_R = 24.3$ min. UV–vis (methanol): λ_{\max}/nm ($\log \epsilon/\text{M}^{-1} \text{cm}^{-1}$) 413 (5.41), 512 (4.02), 548 (3.68), 589 (3.54), 644 (3.34). HRMS: m/z calcd for $\text{C}_{91}\text{H}_{104}\text{N}_{21}\text{O}_{11}$ 1666.82 $[\text{M} + \text{H}]^+$, found 1666.84.

(**2c**) Yield: 50%. HPLC: $t_R = 30.3$ min. UV–vis (methanol): λ_{\max}/nm ($\log \epsilon/\text{M}^{-1} \text{cm}^{-1}$) 378 (4.99), 583 (4.40), 628 (4.53), 650 (4.54). HRMS: m/z calcd for $\text{C}_{144}\text{H}_{186}\text{N}_{37}\text{O}_{25}$ 2833.44 $[\text{M} + \text{H}]^+$, found 2833.39.

(**3c**) Yield: 50%. HPLC: $t_R = 13.7$ min. UV–vis (methanol): λ_{\max}/nm ($\log \epsilon/\text{M}^{-1} \text{cm}^{-1}$) 413 (5.11), 510 (3.81), 544 (3.30), 586 (3.27), 642 (2.89). HRMS: m/z calcd for $\text{C}_{137}\text{H}_{176}\text{N}_{39}\text{O}_{24}$ 2751.37 $[\text{M} + \text{H}]^+$, found 2751.39.

Conjugate 4e. The porphyrin–peptide conjugate **3c** (0.02 mmol), still attached to the solid support, was swelled in DMF, and a 10% solution of methyl iodide in DMF (2 mL) was added to the peptidyl resin. The reaction mixture was shaken overnight at rt and then filtered to remove the excess of reagents. The resin was repeatedly washed with DMF and CH_2Cl_2 and then dried under vacuum. After detachment from the resin, as described above, the conjugate was purified by semipreparative HPLC (linear gradient 17–30% B in 25 min). Yield: 50%. HPLC: $t_R = 12.4$ min. UV–vis (methanol): λ_{\max}/nm ($\log \epsilon/\text{M}^{-1} \text{cm}^{-1}$) 424 (5.15), 515 (3.98), 556 (3.63), 590 (3.51), 647 (3.03). HRMS: m/z calcd for $\text{C}_{141}\text{H}_{187}\text{N}_{39}\text{O}_{24}$ 702.615 $[\text{M}^{++}]$, found 702.874.

Spectroscopic Measurements. Absorption spectra were recorded on a double-beam Cary 6000i spectrophotometer (Varian), equipped with a 110 mm diameter integrating sphere and a high-performance photomultiplier tube for diffuse transmittance measurements. Absorption coefficients were derived from the slopes of Lambert–Beer plots. Fluorescence emission spectra were recorded in a Spex Fluoromax-4 spectrofluorometer. Fluorescence decays were recorded with a time-correlated single-photon-counting system (Fluotime 200) equipped with a red-sensitive photomultiplier. Excitation was achieved by means of a 405 nm LED working at a 10 MHz repetition rate. The counting frequency was always below 1%. Fluorescence decays were analyzed using the PicoQuant FluoFit 4.0 data analysis software. $^1\text{O}_2$ phosphorescence was detected by means of a customized PicoQuant Fluotime 200 system described in detail elsewhere.⁴³ Briefly, a diode-pumped pulsed Nd:YAG laser (FTSS355-Q, Crystal Laser) working at a 10 kHz repetition rate at 532 nm (12 mW, 1.2 μJ per pulse) was used for excitation. A 1064 nm rugate notch filter (Edmund Optics) was placed at the exit port of the laser to remove any residual component of its fundamental emission in the near-IR region. The luminescence exiting from the side of the sample was filtered by a cold mirror (CVI Melles Griot) to remove any scattered laser radiation and focused on the entrance slit of a Science Tech 9055 dual-grating monochromator. A near-IR-sensitive photomultiplier tube assembly (H9170-45, Hamamatsu Photonics) was used as the detector at the exit port of the monochromator. Photon counting was achieved with a multichannel scaler (Becker&Hickl MSA 300 or PicoQuant's Nanoharp 250). The time-resolved emission signals were analyzed using the FluoFit software to extract lifetime values. Laser flash photolysis measurements were carried out using a Q-switched Nd:YAG laser (Surelite I-10, Continuum) with a right-angle geometry and an analyzing beam produced by a Xe lamp (PTI, 75 W) in combination with a dual-grating monochromator (model 101, PTI) coupled to a photomultiplier (Hamamatsu R928). Kinetic analysis of the individual transients was performed with software developed in our laboratory. All spectroscopic measurements were carried out in 1 cm quartz cuvettes (Hellma) at rt. For the

measurements in bacterial suspensions, bacteria were incubated in the dark at the conditions employed for the photoinactivation experiments, namely, 5 μM PS for 1 h. When required, the cells were washed once and resuspended in PBS to a final concentration of $\sim 1 \times 10^7$ cfu mL^{-1} , and 3 mL volumes of the suspensions were irradiated with 3 million laser pulses at 532 nm under gentle stirring. CD measurements were carried out on a Jasco-715 spectropolarimeter, using a quartz cell of 0.1 cm path length. The spectra were recorded at 298 K and were the average of a series of six scans made at 0.1 nm intervals in the 250–190 and 350–550 nm regions. Sample concentrations in water (pH 7), TFE, and aqueous 30 mM SDS were in the range of 10–13 μM . Ellipticity is reported as the mean residue ellipticity $[\theta]_R$ ($\text{deg cm}^2 \text{dmol}^{-1}$).

Bacteria Culture. *E. coli* ATCC 25922 and the methicillin-resistant strain of *S. aureus* ATCC BAA-44 were purchased from LGC Promochem (Teddington, U.K.). Cultures were maintained by two weeks of subcultures in brain heart infusion (BHI; Difco, Detroit, MI) agar. For spectroscopic measurements we used instead the *E. coli* ECT strain, purchased from the Spanish-type cell culture collection.

Bacteria Photoinactivation. For the photoinactivation experiments, the bacteria were grown overnight in BHI at 37 °C, harvested by centrifugation, washed twice, and resuspended in PBS (10 mM phosphate, 0.14 M NaCl, 2.7 mM KCl, pH 7.3) at a density of $\sim 2 \times 10^7$ cells/mL. The cell density was evaluated by measuring the turbidity of the suspension in a Perkin-Elmer spectrophotometer (model Lambda 5). The bacteria used in the experiments were collected from cultures in the stationary phase of growth.

The bacteria were incubated with different concentrations of the PSs in the dark at rt for 60 min or with a fixed PS concentration for different times. After incubation, the suspensions were (i) directly exposed to light with the unbound PS left in the suspension (no washing) or (ii) centrifuged (10000g for 5 min), the pellet resuspended in 1 mL of PBS, and washed two additional times with PBS before illumination (three washings). For illumination, aliquots of cell samples obtained as described above were transferred into 96-well plates (200 $\mu\text{L}/\text{well}$). Samples incubated with porphyrins and its conjugate with apidaecin 1b were irradiated with red light (600–750 nm) with the Waldmann PDT 1200 lamp supplied by Waldmann Medizintechnik; the cells were illuminated from the top of the plates with a fluence rate at the level of the samples of 40 mW/cm^2 , as measured with an International Light power meter, and for a total light dose of 36 J/cm^2 . Bacteria incubated with porphyrins and their conjugates were irradiated with blue light (390–460 nm, with a maximum at 420 nm) emitted by a UV 236 lamp supplied by Waldmann Eclairage SA; the cells were illuminated from the bottom of the plates with a fluence rate of 15.2 mW/cm^2 , as measured with the Waldmann UV-meter, and for a total light dose of 13.5 J/cm^2 . After illumination, aliquots of bacteria suspensions were serially 10-fold-diluted in PBS, and 50 μL volumes of the appropriate dilutions were plated in duplicate onto BHI agar to determine colony-forming units (cfu). Treated and untreated cells were incubated overnight at 37 °C to allow colony formation. Suspensions of bacteria exposed to PSs but kept in the dark and subjected to the same procedure applied to the irradiated suspensions were also plated onto BHI agar after the appropriate serial dilutions. Controls also included bacteria not exposed to any agent and bacteria exposed to light or peptide only. Each experiment was performed at least three times with independent bacterial suspensions.

Flow Cytometry. The interaction of PSs with bacteria was evaluated by flow cytometry. For these experiments, the bacteria were subjected to the same treatments used for photoinactivation experiments, but instead of being illuminated after incubation and washings, they were analyzed with a FACSCanto II flow cytometer. Samples were excited with the 488 nm laser, and fluorescence emission signals were recorded at wavelengths higher than 670 nm. The bacteria population was isolated from the instrument noise by setting electronic gates on the dual-parameter dot plots of forward scatter against side scatter. For each sample, 20 000 events were acquired and analyzed with the FACSDiva software (BD). Samples not incubated with the PSs were used to determine the cell background fluorescence.

■ ASSOCIATED CONTENT

Supporting Information

Fluorescence decay kinetics, singlet oxygen phosphorescence kinetics, and bacteria photoinactivation after repetitive washings and as a function of the incubation time. This material is available free of charge via Internet at <http://pubs.acs.org>.

■ AUTHOR INFORMATION

Corresponding Author

*Phone: +39 0498275741. Fax: +39 0498275829. E-mail: marina.gobbo@unipd.it.

Present Addresses

^{||}Centre for Integrative Bee Research (CIBER), ARC CoE in Plant Energy Biology, MCS Building M316, The University of Western Australia, 6009 Crawley, Australia.

[⊥]Chemistry Research Laboratory, Department of Chemistry, University of Oxford, Mansfield Road, Oxford OX1 3TA, United Kingdom.

Notes

The authors declare no competing financial interest.

■ ACKNOWLEDGMENTS

We thank Dr. Barbara Biondi for ESI-MS analysis. Financial support for this research was obtained from the University of Padova, Progetto di Ateneo 2009 CPDA090338, and from the Spanish Ministerio de Economía y Competitividad through Grants CTQ2010-20870-C03-01 and IT2009-0033. We thank the Italian Ministero dell'Istruzione dell'Università e della Ricerca for Mobility Grant IT10H5E13A. R.R.-G. thanks the Generalitat de Catalunya (DURSI) and Fons Social Europeu for a predoctoral fellowship.

■ ABBREVIATIONS USED

BHI, brain heart infusion; CAMP, cationic antimicrobial peptide; cfu, colony-forming units; D-PBS, deuterated phosphate-buffered saline; PDT, photodynamic therapy; PS, photosensitizer; ROS, reactive oxygen species; TFE, 2,2,2-trifluoroethanol; TMPyP, meso-tetrakis(N-methylpyridinium-yl)porphyrin; TPPS, meso-tetrakis(4-sulfonatophenyl)-porphyrin

■ REFERENCES

- (1) Hamblin, M. R.; Hasan, T. Photodynamic therapy: a new antimicrobial approach to infectious disease? *Photochem. Photobiol. Sci.* **2004**, *3*, 436–450.
- (2) Foote, C. S. Definition of type I and type II photosensitized oxidation. *Photochem. Photobiol.* **1991**, *54*, 659–659.
- (3) Redmond, R.; Gamlin, J. A compilation of singlet oxygen yields from biologically relevant molecules. *Photochem. Photobiol.* **1999**, *70*, 391–475.
- (4) Stark, G. Functional consequences of oxidative membrane damage. *J. Membr. Biol.* **2005**, *205*, 1–16.
- (5) Ravanat, J.; Di Mascio, P.; Martinez, G.; Medeiros, M.; Cadet, J. Singlet oxygen induces oxidation of cellular DNA. *J. Biol. Chem.* **2000**, *275*, 40601–40604.
- (6) Maisch, T. A New strategy to destroy antibiotic resistant microorganisms: antimicrobial photodynamic treatment. *Mini-Rev. Med. Chem.* **2009**, *9*, 974–983.
- (7) Lambrechts, S.; Demidova, T.; Aalders, M.; Hasan, T.; Hamblin, M. Photodynamic therapy for *Staphylococcus aureus* infected burn wounds in mice. *Photochem. Photobiol. Sci.* **2005**, *4*, 503–509.
- (8) Tavares, A.; Carvalho, C. M. B.; Faustino, M. A.; Neves, M. G. P. M. S.; Tome, J. P. C.; Tome, A. C.; Cavaleiro, J. A. S.; Cunha, A.; Gomes, N. C. M.; Alves, E.; Almeida, A. Antimicrobial photodynamic

therapy: study of bacterial recovery viability and potential development of resistance after treatment. *Mar. Drugs* **2010**, *8*, 91–105.

(9) Reddi, E.; Cecon, M.; Valduga, G.; Jori, G.; Bommer, J.; Elisei, F.; Latterini, L.; Mazzucato, U. Photophysical properties and antibacterial activity of meso-substituted cationic porphyrins. *Photochem. Photobiol.* **2002**, *75*, 462–470.

(10) Bertoloni, G.; Rossi, F.; Valduga, G.; Jori, G.; Vanlier, J. Photosensitizing activity of water- and lipid-soluble phthalocyanines on *Escherichia coli*. *FEMS Microbiol. Lett.* **1990**, *71*, 149–155.

(11) Minnock, A.; Vernon, D.; Schofield, J.; Griffiths, J.; Parish, J.; Brown, S. Mechanism of uptake of a cationic water-soluble pyridinium zinc phthalocyanine across the outer membrane of *Escherichia coli*. *Antimicrob. Agents Chemother.* **2000**, *44*, S22–S27.

(12) Tegos, G.; Anbe, M.; Yang, C.; Demidova, T.; Satti, M.; Mroz, P.; Janjua, S.; Gad, F.; Hamblin, M. Protease-stable polycationic photosensitizer conjugates between polyethyleneimine and chlorin-(e6) for broad-spectrum antimicrobial photoinactivation. *Antimicrob. Agents Chemother.* **2006**, *50*, 1402–1410.

(13) Dosselli, R.; Gobbo, M.; Bolognini, E.; Campestrini, S.; Reddi, E. Porphyrin–apidaecin conjugate as a new broad spectrum antimicrobial agent. *ACS Med. Chem. Lett.* **2010**, *1*, 35–38.

(14) Hancock, R. E. W.; Sahl, H. Antimicrobial and host-defense peptides as new anti-infective therapeutic strategies. *Nat. Biotechnol.* **2006**, *24*, 1551–1557.

(15) Otvos, L. The short proline-rich antibacterial peptide family. *Cell. Mol. Life Sci.* **2002**, *59*, 1138–1150.

(16) Li, W.; Ma, G.; Zhou, X. Apidaecin-type peptides: biodiversity, structure-function relationships and mode of action. *Peptides* **2006**, *27*, 2350–2359.

(17) Castle, M.; Nazarian, A.; Yi, S.; Tempst, P. Lethal effects of apidaecin on *Escherichia coli* involve sequential molecular interactions with diverse targets. *J. Biol. Chem.* **1999**, *274*, 32555–32564.

(18) Otvos, L.; O, I.; Rogers, M.; Consolvo, P.; Condie, B.; Lovas, S.; Bulet, P.; Blaszczyk-Thurin, M. Interaction between heat shock proteins and antimicrobial peptides. *Biochemistry* **2000**, *39*, 14150–14159.

(19) Casteels, P.; Romagnolo, J.; Castle, M.; Casteels-Josson, K.; Erdjument-bromage, H.; Tempst, P. Biodiversity of apidaecin-type peptide antibiotics—prospects of manipulating the antibacterial spectrum and combating acquired resistance. *J. Biol. Chem.* **1994**, *269*, 26107–26115.

(20) Taguchi, S.; Mita, K.; Ichinohe, K.; Hashimoto, S. Targeted engineering of the antibacterial peptide apidaecin, based on an in vivo monitoring assay system. *Appl. Environ. Microbiol.* **2009**, *75*, 1460–1464.

(21) Dutta, R. C.; Nagpal, S.; Salunke, D. M. Functional mapping of apidaecin through secondary structure correlation. *Int. J. Biochem. Cell Biol.* **2008**, *40*, 1005–1015.

(22) Zhou, X.; Li, W.; Pan, Y. Functional and structural characterization of apidaecin and its N-terminal and C-terminal fragments. *J. Pept. Sci.* **2008**, *14*, 697–707.

(23) Gobbo, M.; Biondi, L.; Filira, F.; Gennaro, R.; Benincasa, M.; Scolaro, B.; Rocchi, R. Antimicrobial peptides: synthesis and antibacterial activity of linear and cyclic drosocin and apidaecin Ib analogues. *J. Med. Chem.* **2002**, *45*, 4494–4504.

(24) Czihal, P.; Hoffmann, R. Mapping of apidaecin regions relevant for antimicrobial activity and bacterial internalization. *Int. J. Pept. Res. Ther.* **2009**, *15*, 157–164.

(25) Gobbo, M.; Benincasa, M.; Bertoloni, G.; Biondi, B.; Dosselli, R.; Papini, E.; Reddi, E.; Rocchi, R.; Tavano, R.; Gennaro, R. Substitution of the arginine/leucine residues in apidaecin Ib with peptid residues: effect on antimicrobial activity, cellular uptake, and proteolytic degradation. *J. Med. Chem.* **2009**, *52*, 5197–5206.

(26) Matsumoto, K.; Orikasa, Y.; Ichinohe, K.; Hashimoto, S.; Ooi, T.; Taguchi, S. Flow cytometric analysis of the contributing factors for antimicrobial activity enhancement of cell-penetrating type peptides: case study on engineered apidaecins. *Biochem. Biophys. Res. Commun.* **2010**, *395*, 7–10.

- (27) Lindsey, J.; Schereiman, I.; Hsu, H.; Kearney, P.; Marguerettaz, A. Rothemund and Adler–Longo reactions revisited: synthesis of tetraphenylporphyrins under equilibrium conditions. *J. Org. Chem.* **1987**, *52*, 827–836.
- (28) Ishikawa, Y.; Yamashita, A.; Uno, T. Efficient photocleavage of DNA by cationic porphyrin-acridine hybrids with the effective length of diamino alkyl linkage. *Chem. Pharm. Bull.* **2001**, *49*, 287–293.
- (29) Anguera, G.; Llinàs, M. C.; Batllori, X.; Sánchez-García, D. Aryl nitroporphycenes and derivatives: first regioselective synthesis of dinitroporphycenes. *J. Porphyrins Phthalocyanines* **2011**, *15*, 1–6.
- (30) Chan, W. C.; White, P. D. *Fmoc Solid Phase Peptide Synthesis*; Oxford University Press: New York, 2000; pp 41–74.
- (31) Magde, D.; Brannon, J. H.; Cremers, T. L.; Olmsted, J. Absolute luminescence yield of cresyl violet. A standard for the red. *J. Phys. Chem.* **1979**, *83*, 696–699.
- (32) Vergeldt, F. J.; Koehorst, R. B. M.; van Hoek, A.; Schaafsma, T. J. Intramolecular interactions in the ground and excited states of tetrakis(*N*-methylpyridyl)porphyrins. *J. Phys. Chem.* **1995**, *99*, 4397–4405.
- (33) Scaiano, J. C., Ed. *CRC Handbook of Organic Photochemistry*; CRC Press: Boca Raton, FL, 1989; p 496.
- (34) Ogilby, P. R.; Foote, C. S. Chemistry of singlet oxygen. 36. Singlet molecular oxygen ($^1\Delta_g$) luminescence in solution following pulsed laser excitation. Solvent deuterium isotope effects on the lifetime of singlet oxygen. *J. Am. Chem. Soc.* **1982**, *104*, 2069–2070.
- (35) Arai, T.; Inudo, M.; Ishimatsu, T.; Akamatsu, C.; Tokusaki, Y.; Sasaki, T.; Nishino, N. Self-assembling of the porphyrin-linked acyclic penta- and heptapeptides in aqueous trifluoroethanol. *J. Org. Chem.* **2003**, *68*, 5540–5549.
- (36) Sibrian-Vazquez, M.; Jensen, T.; Fronczek, F.; Hammer, R.; Vicente, M. Synthesis and characterization of positively charged porphyrin-peptide conjugates. *Bioconjugate Chem.* **2005**, *16*, 852–863.
- (37) Jori, G. Far-red-absorbing photosensitizers—their use in the photodynamic therapy of tumors. *J. Photochem. Photobiol., A* **1992**, *62*, 371–378.
- (38) Valduga, G.; Breda, B.; Giacometti, G.; Jori, G.; Reddi, E. Photosensitization of wild and mutant strains of *Escherichia coli* by meso-tetra (*N*-methyl-4-pyridyl)porphine. *Biochem. Biophys. Res. Commun.* **1999**, *256*, 84–88.
- (39) George, S.; Hamblin, M. R.; Kishen, A. Uptake pathways of anionic and cationic photosensitizers into bacteria. *Photochem. Photobiol. Sci.* **2009**, *8*, 788–795.
- (40) Dahl, T.; Midden, W.; Hartman, P. Pure singlet oxygen cytotoxicity for bacteria. *Photochem. Photobiol.* **1987**, *46*, 345–352.
- (41) Dai, T.; Huang, Y.; Hamblin, M. R. Photodynamic therapy for localized infections—state of the art. *Photodiagn. Photodyn. Ther.* **2009**, *6*, 170–188.
- (42) Swamy, N.; James, D.; Mohr, S.; Hanson, R.; Ray, R. An estradiol-porphyrin conjugate selectively localizes into estrogen receptor-positive breast cancer cells. *Bioorg. Med. Chem.* **2002**, *10*, 3237–3243.
- (43) Jimenez-Banzo, A.; Ragas, X.; Kapusta, P.; Nonell, S. Time-resolved methods in biophysics. 7. Photon counting vs. analog time-resolved singlet oxygen phosphorescence detection. *Photochem. Photobiol. Sci.* **2008**, *7*, 1003–1010.
- (44) Brown, K. L.; Hancock, R. E. W. Cationic host defense (antimicrobial) peptides. *Curr. Opin. Immunol.* **2006**, *18*, 24–30.
- (45) Tavano, R.; Segat, D.; Gobbo, M.; Papini, E. The honeybee antimicrobial peptide apidaecin differentially immunomodulates human macrophages, monocytes and dendritic cells. *J. Innate Immun.* **2011**, *3*, 614–622.